

Training-Free Global Geometric Association for 4D LiDAR Panoptic Segmentation

Gyeongrok Oh¹, Youngdong Jang¹, Jonghyun Choi², Suk-Ju Kang³,
Guang Lin⁴, and Sangpil Kim^{†,1}

¹ Korea University ²Hyundai Motor Company ³Sogang University ⁴Purdue University

Abstract. Dominant paradigms for 4D LiDAR panoptic segmentation are usually required to train deep neural networks with large superimposed point clouds or design dedicated modules for instance association. However, these approaches perform redundant point processing and consequently become computationally expensive, yet still overlook the rich geometric priors inherently provided by raw point clouds. To this end, we introduce GEO-4D, a simple yet effective training-free framework that unifies spatial and temporal reasoning, enabling holistic LiDAR perception over long time horizons. Specifically, we propose a global geometric association strategy that establishes consistent instance correspondences by estimating an optimal transformation between instance-level point sets. To mitigate instability caused by structural inconsistencies in point cloud observations, we propose a global geometry-aware soft matching mechanism that enforces spatially coherent point-wise correspondences grounded in the spatial distribution of instance point sets. Furthermore, our carefully designed pipeline, which considers three instance types—static, dynamic, and missing—offers computational efficiency and occlusion-aware matching. Our extensive experiments across both SemanticKITTI and nuScenes demonstrate that our method consistently outperforms state-of-the-art approaches, even without additional training or extra point cloud inputs.

1 Introduction

Autonomous driving systems heavily depend on precise perception of dynamic 3D environments with geometrically accurate measurements captured by LiDAR sensors. In particular, LiDAR segmentation plays a crucial role in enabling comprehensive point-wise understanding. In 3D environments, LiDAR panoptic segmentation [19, 35] originates from semantic and instance segmentation, which jointly identify class categories and instance IDs. Along with the recent significant advances in frame-wise perception, 4D LiDAR panoptic segmentation [2] has emerged to capture temporal relationships in a holistic manner. In this context, ensuring temporal continuity is a principal purpose in 4D LiDAR panoptic segmentation, even under instance motions.

[†] Corresponding author.

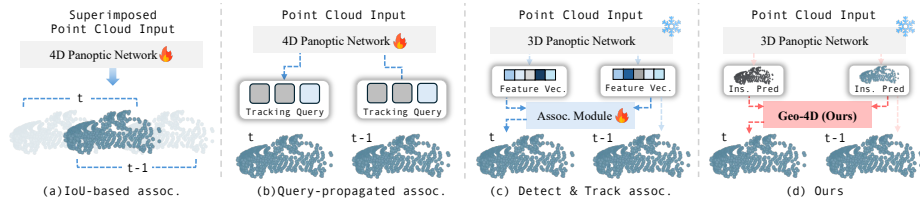


Fig. 1: Comparison of 4D LiDAR panoptic segmentation methods: (a) IoU-based, (b) Query-propagated, (c) Detect & Track, and (d) **Geo-4D**. Instead of relying on training with large-scale point clouds, ours achieves reliable association in a fully training-free manner. 🔥 indicates methods that *require training* and ❄️ denotes *frozen network*.

With its potential benefits, as shown in Figure 1, the mainstream of prior works can be categorized into three discrete paradigms: 1) IoU-based association, 2) Query-propagated association, and 3) Detect & Track association. One solution [2, 15, 20, 58, 67], superimposing point clouds, is widely adopted for establishing 4D spatio-temporal volume. It enables consistent instance tracking over time by measuring overlapping regions (see Figure 1(a)). However, despite its simplicity, stacking point clouds (i.e., increasing the number of points per batch) leads to a quadratic growth in computational overhead, which is an inherent challenge in point cloud processing [22, 31, 54, 55].

An alternative direction [1, 32, 33] seeks to mitigate this issue by treating each scan independently, as illustrated in Figure 1(b) and 1(c). They are primarily derived from the two major paradigms of multi-object tracking, tracking-by-detection [7, 40, 53, 62] and query propagation [34, 59, 63], to assign consistent IDs for instances. Both approaches differ substantially in training strategies, yet commonly suffer from error accumulation [45, 63] and reliance on costly and dataset-dependent training. Consequently, we argue that this suboptimal design fails to fully exploit the strong perceptual capabilities of 3D panoptic networks, which naturally raises the following question: *Can instance association be achieved efficiently using only a 3D panoptic network?*

To answer this, we propose a global geometric association strategy for consistent and reliable instance correspondence, even without any training process. Iterative Closest Point (ICP) is widely used for point cloud registration [11, 50, 61], but its applicability beyond that has been largely underexplored. Here, we integrate ICP into the 4D LiDAR panoptic segmentation framework, thereby enabling explicit instance correspondence through geometric alignment under estimated inter-scan transformations. Additionally, we introduce a novel paradigm for point-wise correspondence, Global Geometry-aware Soft Matching (GGSM), enhancing the robustness to structural noise by enforcing instance-aware geometric correspondences. Traditional ICP performs well on point cloud pairs under ideal conditions, but it relies on nearest-neighbor point correspondences. In real-world noisy measurements acquired from on-vehicle sensors, such point-wise matching often yields incorrect transformations and ultimately leads to erroneous instance associations, as it ignores the global instance structure. In contrast, our GGSM allows reliable correspondences based on the overall geometric context rather than

local proximity. Specifically, it identifies point pairs that minimize the transport cost by solving the earth mover’s problem [12] between two instance point set distributions. As a result, instance association shifts from greedy local pairing to globally consistent alignment, yielding more stable and accurate matching even under challenging environments.

In addition, in real-world observations, instances may remain stationary, move across frames, or temporarily disappear due to occlusion or sensing limitations. Motivated by these instance states, we classify instances into three types: static, dynamic, and missing. For static instances, we apply statistics-based geometric filtering using the mean and covariance of their point distributions to preserve spatial consistency across frames. This filtering step also significantly reduces the number of matching candidates before applying global geometric association to dynamic instances, thereby ensuring computational efficiency. Moreover, we incorporate a short-term memory bank to recover temporarily unobservable instances. We retain only unmatched instances within a short-term window, preserving temporal consistency with minimal memory overhead.

To wrap it up, we named our overall pipeline as **GEO-4D** and demonstrate its effectiveness through extensive experiments on the SemanticKITTI [4] and nuScenes [13] benchmarks. Note that GEO-4D achieves superior performance over existing state-of-the-art methods and ranks 1st on the SemanticKITTI test leaderboard, even under the minimal setting of a single scan and without any additional training.

The contributions of this work are summarized as follows:

- We introduce GEO-4D that is a novel training-free 4D LiDAR panoptic segmentation pipeline, flexibly integrated with a wide range of 3D panoptic segmentation networks.
- We propose a global geometric association strategy to enhance the robustness of instance correspondences, and we delicately design instance state-conditioned solutions to effectively mitigate time complexity and occlusion.
- Extensive experiments in challenging environments clearly demonstrate the superiority of GEO-4D, supported by in-depth analysis.

2 Related Work

LiDAR Panoptic Segmentation. LiDAR panoptic segmentation simultaneously handles two different basis tasks, semantic and instance segmentation. In early, proposal-based methods [30, 37, 56] filter the background points with Mask R-CNN [14]’s semantic head, then group the *thing* points into instances. In contrast, proposal-free methods [16, 25, 41, 66] independently predict semantic prediction and class-agnostic instance segments via end-to-end training manners. 4D LiDAR panoptic segmentation extends these frameworks to sequential scans, requiring instance IDs to remain consistent over time.

In terms of association strategy, predominant works [2, 15, 20, 58, 64, 67] aggregate consecutive point clouds (e.g., 2-4 scans) and group instances in overlapping

regions to ensure temporal continuity. Alternatively, CA-Net [33] associates instances via feature-wise similarity, followed by the outputs of 3D panoptic network. Mask4D [32] preserves identity consistency across scans by iteratively updating the track queries in an end-to-end manner. Despite these attempts, we observe significant issues regarding the computational cost and limited adaptability (see Sec. 1). Instead, we propose GEO-4D that is a flexible, efficient, and well-balanced instance association through direct geometric registration.

Multi-Object Tracking (MOT). MOT is an indispensable task for autonomous driving systems, enabling the tracking of all detected objects across scans. Tracking-by-detection (TBD) paradigm [7, 40, 53, 62] has become the *de facto* standard due to its simplicity and the rapid progress of detectors. Here, the motion model (e.g., Kalman Filter [18]) plays a key role by estimating future object states to maintain tracking continuity. The emergence of DETR [68] has recently drawn increasing attention to the end-to-end paradigm [34, 59, 63], which performs detection and tracking in parallel using query-based tracking. These paradigms are not confined to 2D images but are increasingly embraced in 3D autonomous driving scenarios [39, 52, 60, 65] as well. However, despite sharing objectives with MOT, 4D LiDAR panoptic segmentation differs fundamentally, as it requires holistic point-level scene understanding instead of bounding boxes. Although GEO-4D follows the TBD paradigm, it operates directly on point-level panoptic outputs, enabling instance association grounded in the geometric structure of the underlying point clouds.

Iterative Closest Point (ICP). ICP [6] is one of the most well-established and widely adopted algorithms for point-set registration [9, 24, 43]. Over the years, many variants of the vanilla ICP have been proposed to address its limitations, and have been widely adopted in both traditional engineering [8, 42, 44, 57] and deep learning-based applications [11, 50, 61]. Nowadays, ICP-Flow [29] proposes a compelling scene flow prediction framework that inspired this work. They only consider point-wise motion estimation between two temporally adjacent scans by leveraging well-separated instance clusters. In this paper, we introduce ICP into the context of the 4D LiDAR panoptic segmentation, ensuring the temporal continuity of instances across the entire scans. Remarkably, our Global Geometry-aware Soft Matching enables instance-centric association, even when instance point sets are noisy, imprecise, or fragmented.

3 Method

GEO-4D primarily focuses on ensuring temporal continuity of the instances in a training-free manner. To handle this, we adopt Iterative Closest Point (ICP) [6] to associate instances through their geometric consistency over time. In this section, we first provide a brief introduction to ICP (Sec. 3.1), then go over the technical details of our methods (Sec. 3.2).

3.1 Preliminary

Iterative Closest Point (ICP). Conventionally, for point cloud registration, ICP estimates the optimal transformation by iteratively minimizing the difference between source and target point sets. Given two point sets $\mathcal{P}_{\text{src}} = \{p_1, \dots, p_I\}$ and $\mathcal{P}_{\text{dst}} = \{q_1, \dots, q_J\}$ in \mathbb{R}^3 , it starts with the initial guess of rigid transformation $(\mathbf{R}^{(0)}, \mathbf{t}^{(0)})$, where the rotation $\mathbf{R} \in \text{SO}(3)$ and translation $\mathbf{t} \in \mathbb{R}^3$, which satisfies the following formula:

$$q \approx \mathbf{R}p + \mathbf{t} . \quad (1)$$

Here, in order to compute the alignment error, pairwise correspondences are established using a nearest-neighbor search algorithm (e.g., KD-tree [5]) as:

$$\mathcal{C}^{(k)} = \{(p, \hat{q}) \mid \hat{q} = \arg \min_{q \in \mathcal{P}_{\text{dst}}} \|\mathbf{R}^{(k)}p + \mathbf{t}^{(k)} - q\|, \forall p \in \mathcal{P}_{\text{src}}\}, \quad (2)$$

where k denotes the iteration. Classical ICP adopts l_2 distance as the error metric between the matched point pairs. Ultimately, the optimal rigid transformation is obtained by iteratively solving a series of least-squares problems as:

$$\mathbf{R}^{(k+1)}, \mathbf{t}^{(k+1)} = \arg \min_{\mathbf{R}, \mathbf{t}} \sum_{(p, \hat{q}) \in \mathcal{C}^{(k)}} \|\mathbf{R}p + \mathbf{t} - \hat{q}\|^2 , \quad (3)$$

to update the rotation \mathbf{R} and translation \mathbf{t} until convergence. With this theoretical background, we investigate how ICP contributes to consistent instance ID assignment across frames while enhancing robustness against outliers.

3.2 Geo-4D

Our proposed GEO-4D is developed on top of a pre-trained 3D LiDAR panoptic segmentation model [16, 58], which is specialized in frame-wise perception. Following the standard assumption in LiDAR panoptic segmentation, we transform all points into the world coordinate system using the ego pose. Through this model, we obtain the per-point semantic and instance prediction (s_i, ℓ_i) for a given point cloud, where $s_i \in \{1, \dots, S\}$, $\ell_i \in \mathbb{N}_0$, and S is the number of classes. Prior to the association stage, we construct a set of matching candidates between t and $t - 1$ times by pairing source and destination instances as follows:

$$\mathcal{M} = \mathcal{G}_{\text{src}} \times \mathcal{G}_{\text{dst}} = \{(a, b) \mid a \in \mathcal{G}_{\text{src}}, b \in \mathcal{G}_{\text{dst}}\}, \quad (4)$$

where \mathcal{G}_{src} and \mathcal{G}_{dst} are respectively denoted as the sets of unique instance IDs in the source and destination. Then, we derive the filtered set \mathcal{M}' by keeping only the pairs in \mathcal{M} that share the same semantic class. In this study, we categorize instances into dynamic, static, and missing types to facilitate effective instance association across frames.

Static Instance. Under the assumption that both the center and the shape of a non-moving rigid object remain invariant, we filter static instances based on their centers and further refine them using covariance cues to improve selection

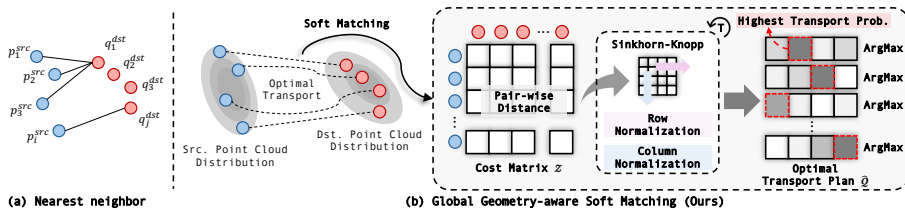


Fig. 2: (a) Nearest neighbor aligns each source point with its closest counterpart, focusing only on local point proximity. (b) In contrast, our Global-Geometry-aware Soft Matching computes correspondences via an optimal transport plan \hat{Q} , enabling instance-aware matching that respects the global geometry of each instance point set.

fidelity. Given the matching candidates \mathcal{M}' , we first represent each instance by the set of 3D points belonging to it. For each instance pair $(a'_{\text{src}}, b'_{\text{dst}}) \in \mathcal{M}'$, we denote the corresponding point sets as $\mathcal{P}(a'_{\text{src}})$ and $\mathcal{P}(b'_{\text{dst}})$, respectively. Then, we compute the centroid of each point set:

$$\mu_s = \frac{1}{|\mathcal{P}(a'_{\text{src}})|} \sum_{p \in \mathcal{P}(a'_{\text{src}})} p, \quad \mu_d = \frac{1}{|\mathcal{P}(b'_{\text{dst}})|} \sum_{q \in \mathcal{P}(b'_{\text{dst}})} q, \quad (5)$$

where $p, q \in \mathbb{R}^3$ represent the world coordinates of points. We keep only the pairs satisfying $\|\mu_d - \mu_s\|_2 < \tau_{\text{center}}$, where τ_{center} is the distance threshold for identifying non-moving objects based on center consistency. Although this naive approach performs well under ideal conditions, it suffers when applied to noisy predicted point sets, resulting in unsuitable pair associations. Thus, we introduce an additional covariance-based constraint that measures the similarity of the spatial spread and geometric structure of the instance point sets. Specifically, the covariance of each point set is computed as follows:

$$\sigma_s = \text{Cov}(\mathcal{P}(a'_{\text{src}})), \quad \sigma_d = \text{Cov}(\mathcal{P}(b'_{\text{dst}})). \quad (6)$$

To assess shape consistency, we measure the similarity between the two covariance matrices and use the predefined threshold τ_{cov} to control the discrepancy between source and destination point set:

$$\frac{\|\sigma_d - \sigma_s\|_F}{\text{tr}(\sigma_d) + \text{tr}(\sigma_s)} < \tau_{\text{cov}}, \quad (7)$$

where $\text{tr}(\cdot)$ and $\|\cdot\|_F$ denote the matrix trace and the Frobenius norm. Then, for all candidate pairs satisfying the filtering conditions, we choose the smallest discrepancy in Eq. 7 for each source instance to determine the best-matching pairs while avoiding duplicate associations.

Dynamic Instance. After filtering static instances, we construct the remaining candidate pair set \mathcal{M}'' . These candidate pairs are then fed into the global geometric association, which serves as the core component of our framework for training-free instance association. In the vanilla ICP loop, the first step is

finding point pairs to compute the distance by utilizing the nearest-neighbor algorithm [5]. While ICP has a powerful ability to register point cloud sets, determining the corresponding points under noisy instance predictions potentially causes erroneous matches. Therefore, we propose a Global Geometry-aware Soft Matching that facilitates stable correspondence estimation within the ICP.

Global Geometry-aware Soft Matching starts by regarding the point cloud as a probability distribution rather than a discrete set of individual points. For a candidate pair $(a''_{\text{src}}, b''_{\text{dst}}) \in \mathcal{M}''$, we denote their corresponding point sets as $\mathcal{P}(a''_{\text{src}}) = \{p_i\}_0^{I-1}$ and $\mathcal{P}(b''_{\text{dst}}) = \{q_j\}_0^{J-1}$, where I and J denote the number of points in each instance. We then formulate the correspondence estimation as an Optimal Transport (OT) problem [12]. Specifically, we seek a transport plan \mathcal{Q} that minimizes the cost of transforming one distribution into the other as follows:

$$\text{OT}(\mathcal{P}(a''_{\text{src}}), \mathcal{P}(b''_{\text{dst}})) := \min_{\mathcal{Q}} \langle \mathcal{Z}, \mathcal{Q} \rangle_F - \epsilon H(\mathcal{Q}), \quad (8)$$

where $\langle \cdot \rangle_F$ denotes Frobenius dot-product. Here, the cost matrix \mathcal{Z} represents the pairwise transport cost, defined as $\mathcal{Z}_{ij} = \|p_i - q_j\|_2^2$. The entropy H and ϵ control the smoothness of the transport plan as a regularization term. Then, we utilize the Sinkhorn-Knopp algorithm [46] that provides an efficient solution to the entropy-regularized optimal transport problem by iteratively rescaling the rows and columns of \mathcal{Q} until the marginal constraints are satisfied (details in supplementary material). Afterwards, we derive the final correspondences from the source to the destination point by taking the argmax operation over each row of the optimal transport plan $\hat{\mathcal{Q}}$ as:

$$j^*(i) = \arg \max_j \hat{\mathcal{Q}}_{ij}, \quad \mathcal{C}_{\text{GGSM}}^{(k)} = \{(p_i, q_{j^*(i)}) \mid i = 0, \dots, I-1\}. \quad (9)$$

That is, we approximate point-to-point correspondences by selecting the highest transport probability from the minimized transport plan. As a result, this strategy is based on considering the instance instead of local points (see Figure 2), thereby alleviating the vulnerability to outliers and incorrect predictions.

Returning to the ICP procedure, we follow the standard process, initializing the transformation with a histogram-based method [29] to reduce sensitivity to initial estimates and subsequently running iterative refinement to get the final rigid transformation. After obtaining the transformation (\mathbf{R}, \mathbf{t}) , we determine whether two instances correspond by evaluating the IoU between their transformed point sets. Specifically, points with errors smaller than the predefined threshold τ_{dist} are treated as inliers. Then, in order to filter valid matching candidates, we evaluate alignment accuracy between source and destination instances using IoU scores as follows:

$$\delta(a''_{\text{src}}, b''_{\text{dst}}) = \mathbb{1}[\text{IoU}(\mathcal{F}(\mathcal{P}(a''_{\text{src}})), \mathcal{P}(b''_{\text{dst}})) \geq \tau_{\text{iou}}], \quad (10)$$

where $\text{IoU}(\cdot)$ denotes the IoU calculation, and \mathcal{F} applies the estimated transformation obtained by ICP. Using Eq. 10, we assign the same instance ID to

matched candidates. In our experiments, this simple matching strategy consistently outperforms more complex assignment schemes. Additional comparisons are provided in the supplementary material.

Missing Instance. Occlusions stemming from the inherent limitations of LiDAR sensor often break temporal continuity beyond two consecutive scans. To mitigate this, we introduce a memory bank \mathcal{B} that caches the world coordinates, semantic labels, and instance IDs of unmatched objects in both static and dynamic association stages. Owing to bounded memory capacity, \mathcal{B} keeps only entries observed within a short window of the previous w_{mem} scans. If \mathcal{B} is not empty, we retrieve the stored instance information and apply the global geometric association strategy to restore temporal consistency.

4 Experiments

4.1 Experiment Setup

Datasets. We choose two representative benchmarks. SemanticKITTI [4] captures point clouds using a 64-beam LiDAR at 10 Hz and provides point-wise annotations for 19 semantic classes (8 Things / 11 Stuff). In contrast, panoptic nuScenes [13] uses a 32-beam LiDAR operating at 2 Hz and offers point-wise annotations for 16 semantic classes (10 Things / 6 Stuff). This contrast serves as a valuable testbed for assessing generalization across dense (SemanticKITTI) and sparse (nuScenes) LiDAR settings.

Evaluation Metrics. To evaluate both tracking and segmentation quality, we adopt the widely used LSTQ metric [2], defined as $\text{LSTQ} = \sqrt{S_{cls} \times S_{assoc}}$. Here, S_{cls} measures how accurately semantic labels are assigned and S_{assoc} evaluates how consistently instance identities are maintained throughout the sequence, independently of semantic accuracy. However, S_{assoc} is computed only from true positive associations weighted by IoU scores. Thus, when prediction masks are stable and yield high IoU scores, ID switch causes a sharper drop in this score. Consequently, while GEO-4D primarily influences S_{assoc} , the LSTQ must be taken into account as a meaningful indicator of temporal consistency.

Implementation Details. Our proposed GEO-4D can be incorporated into any 3D LiDAR panoptic segmentation network. For fair comparison, we basically follow the configurations of two baselines, DS-Net [16] and Mask4Former [58]. Since Mask4Former is originally developed for 4D panoptic segmentation, we train it using the official settings with the input modified to a single scan instead of multiple sweeps. For instance association, thresholds for filtering instance pairs are set to $\tau_{center} = \tau_{cov} = \tau_{dist} = 0.1$ and $\tau_{iou} = 0.2$. Additionally, the short window w_{mem} is set to 3 for missing instances, the regularization parameter for optimal transport is set to $\epsilon = 0.2$, and the number of ICP iterations is fixed to 30. All experiments are conducted on a single RTX A6000.

Table 1: Quantitative results on SemanticKITTI [4]. We highlight the best scores in **bold** and the underline indicates the second-best scores. Note that * represents that the results are obtained from our implementation following the official training setup.

Method	# Scan	Assoc. Training	Validation set				Test set					
			LSTQ	S _{assoc}	S _{cls}	IoU St	IoU Th	LSTQ	S _{assoc}	S _{cls}	IoU St	IoU Th
(a) IoU-based Association												
4D-PLS [2]	4	✗	62.7	65.1	60.5	65.4	61.3	56.9	56.4	57.4	66.9	51.6
4D-StOP [20]	4	✗	67.0	74.4	60.3	65.3	60.9	63.9	69.5	58.8	67.7	53.8
Eq-4D-StOP [67]	4	✗	70.1	<u>77.6</u>	63.4	66.4	67.1	67.0	72.0	62.4	69.1	60.9
Mask4Former [58]	2	✗	70.5	74.3	66.9	67.1	66.6	<u>68.4</u>	67.3	69.6	72.7	65.3
(b) Query-propagated Association												
Mask4D [32]	1	✓	<u>71.4</u>	75.4	67.5	65.8	69.9	64.3	66.4	62.2	69.9	52.2
(c) Detect & Track Association												
KPConv [47]+PP [23]+MOT [51]	1	✓	46.3	37.6	57.0	64.2	54.1	38.0	25.9	55.9	66.9	47.7
KPConv+PP+SFP [36]	1	✓	46.0	37.1	57.0	64.2	54.1	38.5	26.6	55.9	66.9	47.7
DS-Net [16]	1	-	-	-	63.5	64.6	62.0	-	-	60.6	66.9	52.0
+ CA-Net [33]	1	✓	67.4	71.6	63.5	64.6	62.0	62.1	63.7	60.6	66.9	52.0
+ GEO-4D (Ours)	1	✗	68.5 (+1.1)	74.0 (+2.4)	63.5	64.6	62.0	62.9 (+0.8)	65.3 (+1.6)	60.6	66.9	52.0
Mask4Former*	1	-	-	-	67.5	65.2	70.6	-	-	70.5	72.7	67.4
+ CA-Net*	1	✓	70.4	73.4	67.5	65.2	70.6	66.5	62.8	70.5	72.7	67.4
+ GEO-4D (Ours)	1	✗	72.7 (+2.3)	78.3 (+4.9)	67.5	65.2	70.6	70.3 (+3.8)	<u>70.0 (+7.2)</u>	70.5	72.7	67.4

Table 2: Quantitative results on panoptic nuScenes [13].

Method	# Scan	LSTQ	S _{assoc}	S _{cls}	IoU St	IoU Th
(a) IoU-based Association						
4D-StOP [20]	4	60.5	62.5	58.6	74.4	54.9
Eq-4D-StOP [67]	4	67.3	73.7	61.5	76.4	58.7
Mask4Former* [58]	2	<u>67.6</u>	63.0	72.5	76.6	66.3
(b) Query-propagated Association						
Mask4D* [32]	1	58.5	54.1	63.1	75.5	55.7
(c) Detect & Track Association						
Mask4Former*	1	-	-	71.0	76.0	65.9
+ CA-Net*	1	63.4	56.6	71.0	76.0	65.9
+ GEO-4D (Ours)	1	67.9	<u>65.0</u>	71.0	76.0	65.9

Table 3: Comparisons across multiple metrics on SemanticKITTI validation set. () denotes the number of input scans.

Method	LSTQ	MOTSA	sMOTSA	PTQ	sPTQ
4D-StOP* (2f)	66.4	31.0	27.1	53.4	53.7
EQ-4D-StOP* (2f)	68.9	43.6	39.6	56.4	56.7
Mask4D (1f)	71.4	52.1	48.1	58.4	58.5
Mask4Former (2f)	70.5	47.3	42.1	48.3	48.5
Mask4Former* (1f)	-	-	-	-	-
+ CA-Net*	70.4	48.4	43.1	48.9	49.1
+ GEO-4D (Ours)	72.7	73.3	65.7	59.6	59.7

4.2 4D LiDAR Panoptic Segmentation Results

SemanticKITTI. Table 1 reports the experimental results on SemanticKITTI validation and hidden test set. Here, we clearly observe two insights. First, GEO-4D achieves the highest LSTQ score across all data splits regardless of the number of input scans. Specifically, while (a) IoU-based association approaches rely on 2-4 more input point clouds, our GEO-4D achieves superior performance using only a single scan, showing improvements of up to 13.2 percent points in S_{assoc} and 10.0 percent points in LSTQ. Furthermore, by comparing with the learning-based approaches (b) and (c), another noticeable aspect is that GEO-4D consistently outperforms recent state-of-the-art methods on both the validation and test sets, whereas Mask4D and CA-Net drop in performance on the test set. This highlights the robustness of our direct geometric registration with raw point clouds, rather than relying on training-dependent feature association.

nuScenes. Table 2 shows the 4D panoptic results on panoptic nuScenes dataset. Consistent with the observations on the SemanticKITTI, GEO-4D delivers notably stronger instance association performance, outperforming existing methods

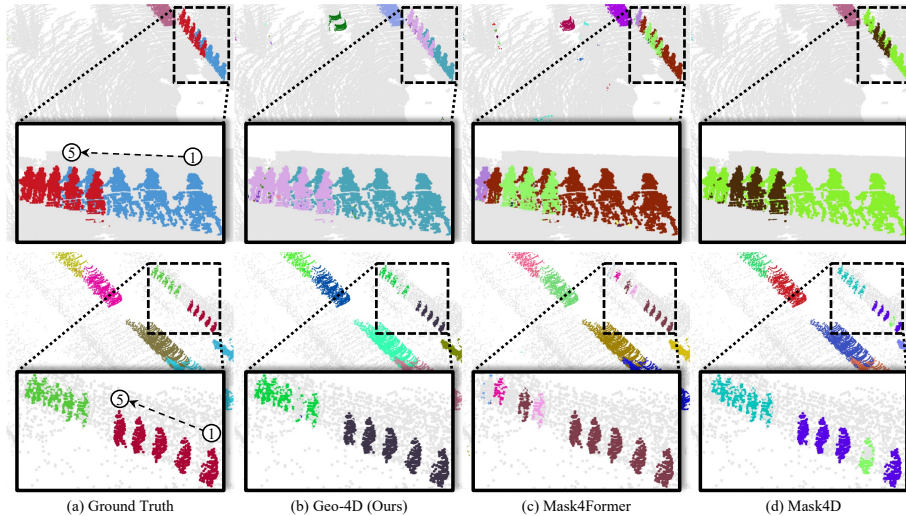


Fig. 3: Qualitative comparison on SemanticKITTI validation set. We visualize the association results over five consecutive scans for both the baselines and our GEO-4D. Different colors represent different instances. The dotted boxes zoom in for clear comparison. For clarity, we use circled numbers (①–⑤) to represent the frame indices.

in terms of LSTQ. It is important to note that baselines generally suffer when the LiDAR scans are captured with a long interval. In such scenarios, multi-scan aggregation benefits from denser temporal support and thus exhibit strong performance. For example, EQ-4D-StOP with 4 aggregated scans surpasses Mask4Former with 2 scans by a substantial margin in the association metric. Nevertheless, GEO-4D demonstrates that even without accessing multiple scans, a single-scan input is sufficient to achieve competitive performance. This result implies that GEO-4D remains highly effective even under sparse LiDAR configurations.

Results on Multiple Metrics. We further present additional results with multiple metrics to enable a more comprehensive comparison. MOTSA [49] is widely used for evaluating multi-object tracking and segmentation. Although MOTSA emphasizes the recognition quality rather than temporal consistency, it nonetheless offers a straightforward indicator of the ID switches. Moreover, PTQ [17] is designed to jointly evaluate panoptic segmentation and tracking quality in a holistic manner. In Table 3, evaluations are carried out on the SemanticKITTI [4] validation set. We observe that GEO-4D consistently surpasses all baselines across multiple metrics, including LSTQ. This indicates that the strength of GEO-4D goes beyond any particular metric, offering a robust and practically reliable solution for instance association.

Comparison of Efficiency. Next, we examine computational efficiency in terms of memory usage and runtime. For each method, we report the peak GPU memory consumption and the average runtime measured over the entire validation set. Figure 4 illustrates the results, supporting that GEO-4D offers the

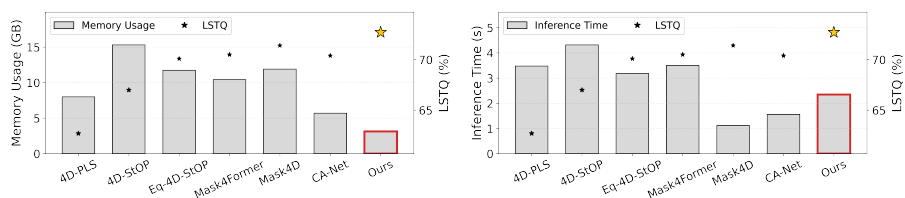


Fig. 4: We illustrate the efficiency trade-offs between memory usage (left) & runtime (right) and performance across different methods.

most well-balanced trade-off between performance and computational overhead. First, when compared with the IoU-based association approaches, we observe that GEO-4D requires 60.7%–79.4% less memory and achieves a 26.1%–45.6% runtime efficiency improvement, all while delivering superior LSTQ performance. While Mask4D exhibits high efficiency in runtime, it inevitably incurs substantial memory overhead due to its transformer-based architecture design. Lastly, CA-Net is computationally efficient; however, it fails to obtain reliable association performance. This gap is already observable on the validation set and becomes even more pronounced on the hidden test set, as highlighted in blue in Table 1.

Qualitative Analysis. We deeply analyze the effectiveness of GEO-4D qualitatively by presenting the visualization results in Figure 3. In the first row, there are two bicyclists riding in a line. Both ground truth and GEO-4D consistently distinguish the two bicyclists across time. However, Mask4Former struggles to preserve identity consistency when objects are spatially adjacent or overlapping due to its IoU-based association. Furthermore, Mask4D employs learnable tracking queries for association, which can lead to confused tracking queries when objects share similar visual or spatial features. Then, in the second row, we emphasize the effectiveness of our memory bank in handling missing instances. Even when the 3D panoptic model fails to detect the person colored in green at the second time step, the memory bank successfully retrieves the missing instance and preserves its identity across scans. In contrast, Mask4Former experiences ID switching when it fails to detect an instance due to the absence of overlapping regions. Consequently, these observations underscore the importance of explicit geometric matching in our approach and a well-structured association pipeline.

4.3 Ablation Study

We conduct a series of ablation studies to validate the effectiveness of each component in our framework. All experiments are performed on the SemanticKITTI [4] validation set, with GEO-4D integrated into Mask4Former [58].

Module Design. Table 4 shows the effects of our proposed methods. Exp. #1 directly applies the vanilla Iterative Closest Point (ICP) for associating instances, serving as a baseline to examine the feasibility of ICP in an unsupervised manner. Despite its strong matching capability, ICP is highly sensitive to the quality

Table 4: Ablation on module design.

Exp. #	Method			Metric	
	Hist. Init.	GGSM	Memory Bank	LSTQ	S _{assoc}
1	-	-	-	70.1	73.4
2	✓	-	-	71.3	75.4
3	-	✓	-	71.4	75.6
4	✓	✓	-	72.0	76.8
5	✓	✓	✓	72.7 (+2.6)	78.3 (+4.9)

Table 5: Ablation study on different types of instances.

Instance Type			Metric		
Static	Dynamic	Missing	LSTQ	S _{assoc}	Inf. time (s)
✓	-	-	35.4	18.5	1.06
-	✓	-	71.8	76.7	3.98
✓	✓	-	72.0	76.8	2.06 $\leftarrow -48.2\%$
✓	✓	✓	72.7	78.3	2.35 $\leftarrow -41.0\%$

of initial alignment. In Exp. #2, we observe a little performance gain when applying histogram-based initialization proposed by [29], which stabilizes the initial alignment. Notably, our Global Geometry-aware Soft Matching (GGSM) brings further improvements without the influence of initial pose (see Exp. #3). The key takeaway is that instance-aware correspondence to alleviate the instability of local point matching is highly beneficial for obtaining reliable matching points between noisy instance segments, and as a result helps to estimate an accurate transformation. Exp. #4 demonstrates that coupling these components yields a complementary effect, leading to more robust instance association and improved overall performance. Lastly, Exp. #5 demonstrates the effectiveness of incorporating a memory bank for handling occluded and missing instances, resulting in superior performance.

Effect of Different Types of Instances. To validate our carefully designed pipeline with respect to different instance types, Table 5 presents the association results and average inference time per a single scan. First, we employ a statistics-based geometric filtering for static instances to match candidates over all detected objects. Despite requiring minimal computation, only a small subset of instances remain consistently tracked, 18.5 percent points indicating that static cues alone are insufficient for reliable association. In contrast, relying solely on global geometry association achieves high performance, but is computationally expensive. Thus, combining these strategies reduces the runtime by 48.2% while simultaneously improving performance, as it significantly narrows the matching candidates for global geometry association. Consequently, our full GEO-4D enhances the tracking continuity without sacrificing computational efficiency.

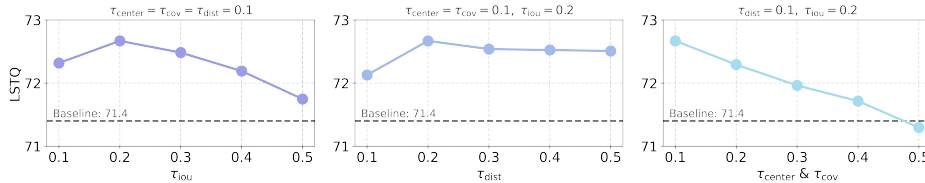


Fig. 5: We illustrate the performance variation w.r.t. the hyperparameters of GEO-4D. The dashed line marks Mask4D, the strongest-performing baseline.

Table 6: DBSCAN instance refinement.

Method	LSTQ	S_{assoc}	S_{cls}	Inf. Time (s)
w/o DBSCAN [10]	71.8	75.8	67.5	0.84
w/ DBSCAN	72.7	78.3	67.5	2.35

Hyperparameter Analysis In this section, we examine the impact of different matching thresholds on instance association performance. We empirically determine the matching thresholds $\{\tau_{iou}, \tau_{dist}, \tau_{center}, \tau_{cov}\}$ over $\{0.1, 0.2, 0.3, 0.4, 0.5\}$. Here, we observe three insights. First, extremely low value of threshold τ_{iou} often yields decent performance due to over-association, whereas high thresholds lead to over-filtering and degraded matching quality. Second, excessively large τ_{center} and τ_{cov} cause static instances to be matched too liberally, leading to unreliable association. Lastly, our proposed GEO-4D delivers performance gains over all baselines, regardless of the hyperparameter choices.

Analysis of DBSCAN Instance Refinement. In this specific experiment of integrating GEO-4D with Mask4Former, we apply DBSCAN clustering [10] as done in the original Mask4Former setting. Table 6 summarizes the results, where we derive two major insights. First, GEO-4D consistently surpasses existing state-of-the-art methods, both with and without the additional clustering step, achieving at least a 0.4 percentage point gain in LSTQ. Furthermore, we discover that the increase of runtime primarily results from the post-processing step. Without this step, GEO-4D delivers the most efficient runtime of 840 ms compared to all other methods, with only a marginal loss in performance. These observations clearly highlight that GEO-4D offers both high efficiency and strong performance, and can further benefit from improvements in the backbone network.

Effect of Global Geometry-aware Soft Matching. The Global Geometry-aware Soft Matching (GGSM) forms instance-aware point correspondence between source and target points. Owing to this strategy, accurate error measurements can be obtained even in the presence of outliers, as the estimation is not dominated by local proximity. Figure 6 visualizes the point-wise correspondences obtained from two consecutive scans, with the current scan serving as the source and the previous scan as the target. For this analysis, we extract each point segment at the initial stage of ICP, as this stage retains its geometric structure intact. As shown in the highlighted region, the nearest-neighbor matching is biased toward the closest point, ignoring the underlying point-wise relationships of the

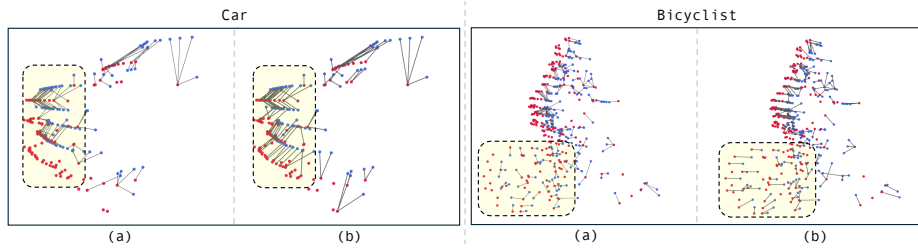


Fig. 6: Visualization of point-wise correspondences. (a) Nearest-neighbor matching. (b) Our Global Geometry-aware Soft Matching. \bullet and \bullet represent the target and source points, respectively.

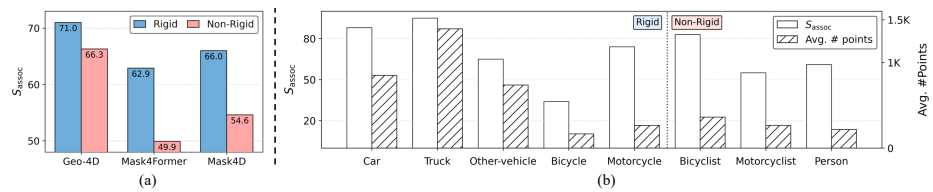


Fig. 7: (a) Comparison with representative baselines across different association strategy categories on rigid and non-rigid object classes. (b) Class-wise performance with respect to object class types and the average number of points per instance.

instance. In contrast, applying GGSM on the baseline maintains the geometric structure, yielding correspondences that align consistently with the instance’s motion direction.

Rigid vs. Non-Rigid Class Analysis. We categorize object classes into rigid (car, truck, other-vehicle, bicycle, motorcycle) and non-rigid (bicyclist, motorcyclist, person) groups based on their physical characteristics. As shown in Figure 7(a), GEO-4D outperforms representative IoU-based and query-based association baselines across both rigid and non-rigid classes. Furthermore, GEO-4D consistently maintains strong association performance across all object classes (see Figure 7(b)). These results are attributed to the robustness of our proposed global geometry-aware association strategy, which captures holistic geometric structure and enables reliable association under partial non-rigid motion and significant variations in object size.

5 Conclusion

In this paper, we introduce a novel instance association strategy GEO-4D for 4D LiDAR panoptic segmentation, the first training-free framework tailored for a single scan setting. Our proposed Global Geometry-aware Soft Matching forming instance-aware correspondence enables ICP procedure to precisely align between two consecutive instance point segments, thereby improving temporal continuity. Additionally, we systematically design the overall pipeline, underscoring the instance types to alleviate the inherent challenges of ICP and LiDAR sensors.

Through experimental evaluations on both SemanticKITTI and nuScenes, our GEO-4D showcases its superiority not only on the validation sets but also on the hidden test sets, demonstrating robustness across various sensor configurations. Ultimately, our approach offers a promising direction for 4D perception by solely leveraging strong 3D panoptic models to support temporal understanding.

Limitations. Although GEO-4D shows substantial promise in advancing 4D perception, several limitations persist that warrant further investigation, particularly in real-time deployment, handling partial LiDAR observations, and dependence on accurate ego pose estimation. We provide additional discussions in the supplementary materials.

References

1. Athar, A., Li, E., Casas, S., Urtasun, R.: 4d-former: Multimodal 4d panoptic segmentation. In: Conference on Robot Learning. pp. 2151–2164. PMLR (2023)
2. Aygun, M., Osep, A., Weber, M., Maximov, M., Stachniss, C., Behley, J., Leal-Taixe, L.: 4d panoptic lidar segmentation. In: Proceedings of the IEEE/CVF Conference on Computer Vision and Pattern Recognition (CVPR). pp. 5527–5537 (June 2021)
3. Bazaraa, M.S., Jarvis, J.J., Sherali, H.D.: Linear programming and network flows. John Wiley & Sons (2011)
4. Behley, J., Garbade, M., Milioto, A., Quenzel, J., Behnke, S., Stachniss, C., Gall, J.: Semantickitti: A dataset for semantic scene understanding of lidar sequences. In: Proceedings of the IEEE/CVF international conference on computer vision. pp. 9297–9307 (2019)
5. Bentley, J.L.: Multidimensional binary search trees used for associative searching. Communications of the ACM **18**(9), 509–517 (1975)
6. Besl, P.J., McKay, N.D.: Method for registration of 3-d shapes. In: Sensor fusion IV: control paradigms and data structures. vol. 1611, pp. 586–606. Spie (1992)
7. Bewley, A., Ge, Z., Ott, L., Ramos, F., Upcroft, B.: Simple online and realtime tracking. In: 2016 IEEE international conference on image processing (ICIP). pp. 3464–3468. Ieee (2016)
8. Bouaziz, S., Tagliasacchi, A., Pauly, M.: Sparse iterative closest point. In: Computer graphics forum. vol. 32, pp. 113–123. Wiley Online Library (2013)
9. Bustos, A.P., Chin, T.J.: Guaranteed outlier removal for point cloud registration with correspondences. IEEE transactions on pattern analysis and machine intelligence **40**(12), 2868–2882 (2017)
10. Campello, R.J., Moulavi, D., Sander, J.: Density-based clustering based on hierarchical density estimates. In: Pacific-Asia conference on knowledge discovery and data mining. pp. 160–172. Springer (2013)
11. Choy, C., Dong, W., Koltun, V.: Deep global registration. In: Proceedings of the IEEE/CVF conference on computer vision and pattern recognition. pp. 2514–2523 (2020)
12. Cuturi, M.: Sinkhorn distances: Lightspeed computation of optimal transport. Advances in neural information processing systems **26** (2013)
13. Fong, W.K., Mohan, R., Hurtado, J.V., Zhou, L., Caesar, H., Beijbom, O., Valada, A.: Panoptic nusenes: A large-scale benchmark for lidar panoptic segmentation and tracking. IEEE Robotics and Automation Letters **7**(2), 3795–3802 (2022)

14. He, K., Gkioxari, G., Dollár, P., Girshick, R.: Mask r-cnn. In: Proceedings of the IEEE international conference on computer vision. pp. 2961–2969 (2017)
15. Hong, F., Kong, L., Zhou, H., Zhu, X., Li, H., Liu, Z.: Unified 3d and 4d panoptic segmentation via dynamic shifting networks. *IEEE Transactions on Pattern Analysis and Machine Intelligence* **46**(5), 3480–3495 (2024). <https://doi.org/10.1109/TPAMI.2023.3349304>
16. Hong, F., Zhou, H., Zhu, X., Li, H., Liu, Z.: Lidar-based panoptic segmentation via dynamic shifting network. In: Proceedings of the IEEE/CVF conference on computer vision and pattern recognition. pp. 13090–13099 (2021)
17. Hurtado, J.V., Mohan, R., Burgard, W., Valada, A.: Mopt: Multi-object panoptic tracking. arXiv preprint arXiv:2004.08189 (2020)
18. Kalman, R.E.: A new approach to linear filtering and prediction problems (1960)
19. Kirillov, A., He, K., Girshick, R., Rother, C., Dollár, P.: Panoptic segmentation. In: Proceedings of the IEEE/CVF conference on computer vision and pattern recognition. pp. 9404–9413 (2019)
20. Kreuzberg, L., Zufikar, I.E., Mahadevan, S., Engelmann, F., Leibe, B.: 4d-stop: Panoptic segmentation of 4d lidar using spatio-temporal object proposal generation and aggregation. In: European Conference on Computer Vision. pp. 537–553. Springer (2022)
21. Kuhn, H.W.: The hungarian method for the assignment problem. *Naval research logistics quarterly* **2**(1-2), 83–97 (1955)
22. Lai, X., Liu, J., Jiang, L., Wang, L., Zhao, H., Liu, S., Qi, X., Jia, J.: Stratified transformer for 3d point cloud segmentation. In: Proceedings of the IEEE/CVF conference on computer vision and pattern recognition. pp. 8500–8509 (2022)
23. Lang, A.H., Vora, S., Caesar, H., Zhou, L., Yang, J., Beijbom, O.: Pointpillars: Fast encoders for object detection from point clouds. In: Proceedings of the IEEE/CVF conference on computer vision and pattern recognition. pp. 12697–12705 (2019)
24. Li, J.: A practical $o(n^2)$ outlier removal method for correspondence-based point cloud registration. *IEEE Transactions on Pattern Analysis and Machine Intelligence* **44**(8), 3926–3939 (2021)
25. Li, J., He, X., Wen, Y., Gao, Y., Cheng, X., Zhang, D.: Panoptic-phnet: Towards real-time and high-precision lidar panoptic segmentation via clustering pseudo heatmap. In: Proceedings of the IEEE/CVF conference on computer vision and pattern recognition. pp. 11809–11818 (2022)
26. Li, X., Kaesemodel Pontes, J., Lucey, S.: Neural scene flow prior. *Advances in neural information processing systems* **34**, 7838–7851 (2021)
27. Li, Y., Harada, T.: Leopard: Learning partial point cloud matching in rigid and deformable scenes. In: Proceedings of the IEEE/CVF conference on computer vision and pattern recognition. pp. 5554–5564 (2022)
28. Li, Y., Harada, T.: Non-rigid point cloud registration with neural deformation pyramid. *Advances in Neural Information Processing Systems* **35**, 27757–27768 (2022)
29. Lin, Y., Caesar, H.: Icp-flow: Lidar scene flow estimation with icp. In: Proceedings of the IEEE/CVF Conference on Computer Vision and Pattern Recognition. pp. 15501–15511 (2024)
30. Liu, H., Peng, C., Yu, C., Wang, J., Liu, X., Yu, G., Jiang, W.: An end-to-end network for panoptic segmentation. In: Proceedings of the IEEE/CVF conference on computer vision and pattern recognition. pp. 6172–6181 (2019)
31. Liu, Z., Yang, X., Tang, H., Yang, S., Han, S.: Flatformer: Flattened window attention for efficient point cloud transformer. In: Proceedings of the IEEE/CVF conference on computer vision and pattern recognition. pp. 1200–1211 (2023)

32. Marcuzzi, R., Nunes, L., Wiesmann, L., Marks, E., Behley, J., Stachniss, C.: Mask4d: End-to-end mask-based 4d panoptic segmentation for lidar sequences. *IEEE Robotics and Automation Letters* **8**(11), 7487–7494 (2023)
33. Marcuzzi, R., Nunes, L., Wiesmann, L., Vizzo, I., Behley, J., Stachniss, C.: Contrastive instance association for 4d panoptic segmentation using sequences of 3d lidar scans. *IEEE Robotics and Automation Letters* **7**(2), 1550–1557 (2022)
34. Meinhardt, T., Kirillov, A., Leal-Taixe, L., Feichtenhofer, C.: Trackformer: Multi-object tracking with transformers. In: *Proceedings of the IEEE/CVF conference on computer vision and pattern recognition*. pp. 8844–8854 (2022)
35. Milioto, A., Behley, J., McCool, C., Stachniss, C.: Lidar panoptic segmentation for autonomous driving. In: *2020 IEEE/RSJ International Conference on Intelligent Robots and Systems (IROS)*. pp. 8505–8512. IEEE (2020)
36. Mittal, H., Okorn, B., Held, D.: Just go with the flow: Self-supervised scene flow estimation. In: *Proceedings of the IEEE/CVF conference on computer vision and pattern recognition*. pp. 11177–11185 (2020)
37. Mohan, R., Valada, A.: Efficientps: Efficient panoptic segmentation. *International Journal of Computer Vision* **129**(5), 1551–1579 (2021)
38. Newcombe, R.A., Fox, D., Seitz, S.M.: Dynamicfusion: Reconstruction and tracking of non-rigid scenes in real-time. In: *Proceedings of the IEEE conference on computer vision and pattern recognition*. pp. 343–352 (2015)
39. Pang, Z., Li, Z., Wang, N.: Simpletrack: Understanding and rethinking 3d multi-object tracking. In: *European Conference on Computer Vision*. pp. 680–696. Springer (2022)
40. Qin, Z., Wang, L., Zhou, S., Fu, P., Hua, G., Tang, W.: Towards generalizable multi-object tracking. In: *Proceedings of the IEEE/CVF Conference on Computer Vision and Pattern Recognition*. pp. 18995–19004 (2024)
41. Razani, R., Cheng, R., Li, E., Taghavi, E., Ren, Y., Bingbing, L.: Gp-s3net: Graph-based panoptic sparse semantic segmentation network. In: *Proceedings of the IEEE/CVF international conference on computer vision*. pp. 16076–16085 (2021)
42. Rusinkiewicz, S., Levoy, M.: Efficient variants of the icp algorithm. In: *Proceedings third international conference on 3-D digital imaging and modeling*. pp. 145–152. IEEE (2001)
43. Rusu, R.B., Blodow, N., Beetz, M.: Fast point feature histograms (fpfh) for 3d registration. In: *2009 IEEE international conference on robotics and automation*. pp. 3212–3217. IEEE (2009)
44. Segal, A., Haehnel, D., Thrun, S.: Generalized-icp. In: *Robotics: science and systems*. vol. 2, p. 435. Seattle, WA (2009)
45. Segu, M., Piccinelli, L., Li, S., Yang, Y.H., Schiele, B., Van Gool, L.: Samba: Synchronized set-of-sequences modeling for multiple object tracking. *arXiv preprint arXiv:2410.01806* (2024)
46. Sinkhorn, R.: Diagonal equivalence to matrices with prescribed row and column sums. *The American Mathematical Monthly* **74**(4), 402–405 (1967)
47. Thomas, H., Qi, C.R., Deschaud, J.E., Marcotegui, B., Goulette, F., Guibas, L.J.: Kpconv: Flexible and deformable convolution for point clouds. In: *Proceedings of the IEEE/CVF international conference on computer vision*. pp. 6411–6420 (2019)
48. Villani, C., et al.: *Optimal transport: old and new*, vol. 338. Springer (2008)
49. Voigtlaender, P., Krause, M., Osep, A., Luiten, J., Sekar, B.B.G., Geiger, A., Leibe, B.: Mots: Multi-object tracking and segmentation. In: *Proceedings of the IEEE/CVF conference on computer vision and pattern recognition*. pp. 7942–7951 (2019)

50. Wang, Y., Solomon, J.M.: Deep closest point: Learning representations for point cloud registration. In: Proceedings of the IEEE/CVF international conference on computer vision. pp. 3523–3532 (2019)
51. Weng, X., Wang, J., Held, D., Kitani, K.: 3d multi-object tracking: A baseline and new evaluation metrics. In: 2020 IEEE/RSJ International Conference on Intelligent Robots and Systems (IROS). pp. 10359–10366. IEEE (2020)
52. Weng, X., Wang, J., Held, D., Kitani, K.: Ab3dmot: A baseline for 3d multi-object tracking and new evaluation metrics. arXiv preprint arXiv:2008.08063 (2020)
53. Wojke, N., Bewley, A., Paulus, D.: Simple online and realtime tracking with a deep association metric. In: 2017 IEEE international conference on image processing (ICIP). pp. 3645–3649. IEEE (2017)
54. Wu, X., Jiang, L., Wang, P.S., Liu, Z., Liu, X., Qiao, Y., Ouyang, W., He, T., Zhao, H.: Point transformer v3: Simpler faster stronger. In: Proceedings of the IEEE/CVF conference on computer vision and pattern recognition. pp. 4840–4851 (2024)
55. Wu, X., Lao, Y., Jiang, L., Liu, X., Zhao, H.: Point transformer v2: Grouped vector attention and partition-based pooling. *Advances in Neural Information Processing Systems* **35**, 33330–33342 (2022)
56. Xiong, Y., Liao, R., Zhao, H., Hu, R., Bai, M., Yumer, E., Urtasun, R.: Upsnet: A unified panoptic segmentation network. In: Proceedings of the IEEE/CVF conference on computer vision and pattern recognition. pp. 8818–8826 (2019)
57. Yang, J., Li, H., Campbell, D., Jia, Y.: Go-icp: A globally optimal solution to 3d icp point-set registration. *IEEE transactions on pattern analysis and machine intelligence* **38**(11), 2241–2254 (2015)
58. Yilmaz, K., Schult, J., Nekrasov, A., Leibe, B.: Mask4former: Mask transformer for 4d panoptic segmentation. In: 2024 IEEE International Conference on Robotics and Automation (ICRA). pp. 9418–9425. IEEE (2024)
59. Zeng, F., Dong, B., Zhang, Y., Wang, T., Zhang, X., Wei, Y.: Motr: End-to-end multiple-object tracking with transformer. In: European conference on computer vision. pp. 659–675. Springer (2022)
60. Zhang, T., Chen, X., Wang, Y., Wang, Y., Zhao, H.: Mutr3d: A multi-camera tracking framework via 3d-to-2d queries. In: Proceedings of the IEEE/CVF Conference on Computer Vision and Pattern Recognition. pp. 4537–4546 (2022)
61. Zhang, X., Yang, J., Zhang, S., Zhang, Y.: 3d registration with maximal cliques. In: Proceedings of the IEEE/CVF conference on computer vision and pattern recognition. pp. 17745–17754 (2023)
62. Zhang, Y., Sun, P., Jiang, Y., Yu, D., Weng, F., Yuan, Z., Luo, P., Liu, W., Wang, X.: Bytetrack: Multi-object tracking by associating every detection box. In: European conference on computer vision. pp. 1–21. Springer (2022)
63. Zhang, Y., Wang, T., Zhang, X.: Motrv2: Bootstrapping end-to-end multi-object tracking by pretrained object detectors. In: Proceedings of the IEEE/CVF conference on computer vision and pattern recognition. pp. 22056–22065 (2023)
64. Zhang, Y., Ošep, A., Leal-Taixé, L., Meinhardt, T.: Zero-shot 4d lidar panoptic segmentation. In: Proceedings of the Computer Vision and Pattern Recognition Conference. pp. 24506–24517 (2025)
65. Zhou, X., Koltun, V., Krähenbühl, P.: Tracking objects as points. In: European conference on computer vision. pp. 474–490. Springer (2020)
66. Zhou, Z., Zhang, Y., Foroosh, H.: Panoptic-polarnet: Proposal-free lidar point cloud panoptic segmentation. In: Proceedings of the IEEE/CVF conference on computer vision and pattern recognition. pp. 13194–13203 (2021)

67. Zhu, M., Han, S., Cai, H., Borse, S., Ghaffari, M., Porikli, F.: 4d panoptic segmentation as invariant and equivariant field prediction. In: Proceedings of the IEEE/CVF International Conference on Computer Vision. pp. 22488–22498 (2023)
68. Zhu, X., Su, W., Lu, L., Li, B., Wang, X., Dai, J.: Deformable detr: Deformable transformers for end-to-end object detection. arXiv preprint arXiv:2010.04159 (2020)

Contents

A	Implementation Details	20
A.1	Baseline Details	20
A.2	Metrics	21
B	Method Details	22
B.1	Pipeline Details	22
B.2	Complexity Analysis	22
B.3	Option: Bijective assignment.	23
C	Additional Experimental Results	24
C.1	Leaderboard Results	24
C.2	Effect of the Number of Scans.	24
C.3	Analysis of Matching Strategy.	25
C.4	Analysis of Global Geometry-aware Soft Matching.	25
C.5	Quantitative Results	27
C.6	Qualitative Results	27
D	Discussion	28
D.1	Limitation and Future work	28

A Implementation Details

A.1 Baseline Details

In this section, we provide a detailed overview of the strong baselines considered in our comparison: 4D-PLS [2] (CVPR’21), 4D-Stop (ECCVW’22) [20], EQ-4D-Stop (ICCV’23) [67], CA-Net (R-AL’22) [33], Mask4D (R-AL’23) [32], and Mask4Former (ICRA’24) [58]. Note that we report the official results as stated in the original papers, and reproduce the results when formal reports are not available. The following paragraph details the experimental settings and notable modifications for each baseline.

First, 4D-PLS, 4D-Stop, and EQ-4D-Stop follow a two-stage design, where instance tracklets are first generated independently for all scans and then stitched across consecutive frames. Accordingly, we measure the inference time of each stage separately and report their average as the overall runtime. Second, Mask4Former is originally developed for 4D LiDAR panoptic segmentation with superimposed point clouds. To establish a strong baseline for our experiments, we train it as a 3D panoptic network without any modifications, except setting the number of input scans to one. Third, CA-Net employs contrastive learning for instance association on top of an off-the-shelf 3D panoptic segmentation network. For a fair comparison, we integrate the single scan Mask4Former into the CA-Net framework. Since CA-Net requires point-wise instance features for contrastive learning, we extract them by computing the dot product between instance queries and instance masks. Lastly, official panoptic nuScenes results are unavailable for any methods except 4D-Stop and EQ-4D-Stop. Therefore, we additionally reproduce the remaining baselines using their official repositories, following the experimental protocol of EQ-4D-StOP.

A.2 Metrics

We provide detailed explanations of the metrics employed for evaluating association performance in our experiments. While LSTQ is the most widely used metric, we additionally report two complementary metrics, MOTSA and PTQ, to provide a more comprehensive assessment.

LSTQ [2] is delicately designed to evaluate 4D panoptic segmentation quality. First, to assess the semantic segmentation performance over the classes C , the classification score S_{cls} is defined as:

$$S_{cls} = \frac{1}{|C|} \sum_{c=1}^C \frac{|\text{TP}_c|}{|\text{TP}_c| + |\text{FN}_c| + |\text{FP}_c|} = \frac{1}{C} \sum_{c=1}^C \text{IoU}(c), \quad (11)$$

where TP, FN, and FP denote the true positives, false negatives, and false positives, respectively. Furthermore, the association score S_{assoc} , which is responsible for measuring temporal continuity, is defined as:

$$S_{assoc} = \frac{1}{|I|} \sum_{t \in I} \frac{1}{|gt_{id}(t)|} \sum_{s \in S, s \cap t \neq \emptyset} \text{TPA}(s, t) \text{IoU}(s, t), \quad (12)$$

where I and S refer to the ground-truth and predicted segments. Note that TPA represents the points that maintain consistent identities across scans, regardless of class. Consequently, LSTQ is computed as the geometric mean of the classification score S_{cls} and association score S_{assoc} .

MOTSA & sMOTSA [49] are mask-based variants of the widely used Multi-Object Tracking Accuracy (MOTA) metric, replacing bounding-box overlaps with mask IoU to better evaluate segmentation-level tracking performance. Formally,

$$\text{MOTSA} = \frac{|\text{TP}| - |\text{FP}| - |\text{IDSW}|}{|M|}, \quad (13)$$

where $|\text{IDSW}|$ denotes the total number of ID switches, and $|M|$ is the number of ground truth segmentation masks. In addition, sMOTSA replaces the true positive (TP) with soft true positive ($s\text{TP}$), obtained by accumulating the mask IoUs over all matched predictions.

PTQ & sPTQ [17] are formulated to satisfy the fundamental requirement that panoptic tracking metrics must jointly capture segmentation accuracy and tracking consistency over time. Thus, they incorporate an ID-switch penalty into the original Panoptic Quality (PQ) measure, as follows:

$$\text{PTQ} = \frac{1}{|C|} \sum_{c=1}^C \frac{\sum_{(s,t) \in \text{TP}_c} \text{IoU}(s, t) - |\text{IDSW}_c|}{|\text{TP}_c| + \frac{1}{2}|\text{FP}_c| + \frac{1}{2}|\text{FN}_c|}. \quad (14)$$

Furthermore, sPTQ leverages the soft version of IDSW (sIDSW) instead of IDSW. This soft variant aggregates the IoU scores for segments in which the predicted instance ID ID changes:

$$s\text{IDSW}_c = \{\text{IoU}(s, t) \mid (s, t) \in \text{TP}_c \wedge ID_s \neq ID_t\}. \quad (15)$$

Algorithm 1 Overall pipeline of GEO-4D

Require: Panoptic prediction (s, l) , memory bank \mathcal{B}

- 1: **for** sequence $t \in \{1, 2, \dots, T - 1\}$ **do**
- 2: Construct the candidate set \mathcal{M}' filtered by semantic predictions s .
 // **Static instances**
- 3: Associate instances using the centroid μ of each point set (Eq. 5).
- 4: Refine the matched pairs using the covariance descriptor σ (Eq. 7).
 // **Dynamic instances**
- 5: Perform global geometric association using ICP enhanced with global geometry-aware soft matching.
 // **Missing instances**
- 6: **if** \mathcal{B} is not empty **then**
- 7: Apply the dynamic matching procedure (Line 5) to missing instances.
- 8: **end if**
- 9: Update the memory bank \mathcal{B} .
- 10: **end for**

Ensure: Consistent instance IDs throughout the entire sequence.

Table A.1: Comparison Between Nearest Neighbor and Global Geometry-aware Soft Matching (GGSM). We report the results of our full Geo-4D when integrating each correspondence strategy.

w/ Nearest Neighbor		w/ GGSM (Ours)	
LSTQ	Inf. Time (s)	LSTQ	Inf. Time (s)
72.1	2.01	72.7	2.35

B Method Details

B.1 Pipeline Details

The overall association pipeline of our proposed GEO-4D is summarized in Algorithm 1. We apply GEO-4D sequentially across all scans within each sequence, and reset the memory bank \mathcal{B} at the beginning of every new sequence.

B.2 Complexity Analysis

In this section, we provide a computational complexity comparison between Global Geometry-aware Soft Matching (GGSM) and nearest neighbor-based matching. As described in the main manuscript, we utilize the entropy-regularized optimal transport problem [12] to obtain instance-aware point correspondences. Before analyzing the regularized form, we briefly review the optimal transport problem. Given two probability vectors $r \in \mathbb{R}_+^n$ and $c \in \mathbb{R}_+^m$, the original optimal transport problem [48] aims to find the optimal transport plan $Q \in U(r, c)$. The entries of Q represent the amount of mass transported from the i -th element of r to the

j -th element of c . The transport polytope U is defined as:

$$U(r, c) = \{Q \in \mathbb{R}_+^{n \times m} \mid \sum_j Q_{ij} = r_i, \forall i, \sum_i Q_{ij} = c_j, \forall j\}. \quad (16)$$

Let \mathcal{Z} denote the transport cost matrix. The optimal transport plan is then computed as the Frobenius inner product between \mathcal{Q} and \mathcal{Z} :

$$\text{OT}(r, c) := \min_{\mathcal{Q}} \langle \mathcal{Z}, \mathcal{Q} \rangle_F. \quad (17)$$

This optimization is a linear program, for which the network simplex [3] is the most widely used exact solver. In the symmetric case $n = m$, its worst-case computational complexity scales as $O(n^3 \log n)$. However, due to its heavy computational cost, adding an entropic regularization is widely adopted to accelerate optimal transport. By incorporating the Shannon entropy $H(\mathcal{Q}) := -\sum_{i,j} \mathcal{Q}_{ij} \log \mathcal{Q}_{ij}$ into Eq. 17, we obtain the entropy-regularized optimal transport formulation. To handle marginal constraints, we introduce dual variables $f \in \mathbb{R}^n$ and $g \in \mathbb{R}^m$ and form the corresponding Lagrangian. Then, by taking the first-order optimality condition, we find that optimal solution $\hat{\mathcal{Q}}$ has matrix form $\hat{\mathcal{Q}} = \text{diag}(u)K\text{diag}(v)$, where $u_i = e^{f_i/\epsilon}$, $v_j = e^{g_j/\epsilon}$, and $K_{ij} = e^{-Z_{ij}/\epsilon}$. Since u and v must satisfy the marginal constraints, the entropic regularization transforms the classical optimal transport problem from a linear program into a matrix scaling problem. Thus, when $n = m$, the computational complexity is reduced to $O(n^2)$. However, the nearest neighbor algorithm operates in $O(n \log n)$ on average and up to $O(n^2)$ in the worst case in practice, as implemented in the scikit-learn library (e.g., using KD-Tree [5]). Consequently, our GGSM solution is theoretically comparable to the nearest neighbor algorithm, and the wall-clock time shows only a marginal difference while achieving higher performance (see Table A.1).

B.3 Option: Bijective assignment.

As mentioned in the main manuscript, our simple heuristic matching strategy consistently outperforms more complex assignment schemes, despite its simplicity. Here, we provide additional comparisons and describe an alternative bijective assignment formulation. A naive approach in global geometric association maintains consistent instance identities by assigning a single instance ID to matched candidates; however, this fails to enforce one-to-one correspondence. Thus, we derive a transformation-aware matching cost that integrates the global geometric association results—rotation \mathbf{R} , translation \mathbf{t} , and the IoU score s_{iou} . Formally, the matching cost \mathcal{C} of dynamic matching pairs $(i, j) \in \mathcal{M}''$ is defined as:

$$\begin{aligned} \mathcal{C}_{ij} &= \gamma_t c_{ij}^{(t)} + \gamma_r c_{ij}^{(r)} + \gamma_s c_{ij}^{(s)}, \\ c_{ij}^{(t)} &= \|\mathbf{t}_{ij}\|_2, \quad c_{ij}^{(r)} = \|\theta_{ij}\|_2, \quad c_{ij}^{(s)} = \|1 - s_{iou}\|_2, \end{aligned} \quad (18)$$

where θ denotes the axis-angle rotation vector obtained from \mathbf{R} . We normalize each cost term to comparable scales before weighting so that γ_t , γ_r , and γ_s control

Table A.2: SemanticKITTI [4] Test Set Leaderboard (Top 5). mAQ and mIoU denote S_{assoc} and S_{cls} , respectively.

Rank	User	LSTQ \uparrow	mAQ \uparrow	mIoU \uparrow
1	GEO-4D (Ours)	70.3	70.0	70.5
2	guysh	70.2	70.6	69.7
2	YAKD	68.6	70.8	66.5
3	hphnngcquan	68.5	70.4	66.7
4	KadirYilmaz	68.4	67.3	69.6

Table A.3: Analysis on performance over the number of superimposed scans.

Method	# Scan	Memory (GB)	Time (s)	Validation set					Test set				
				LSTQ	S_{assoc}	S_{cls}	IoU^{St}	IoU^{Th}	LSTQ	S_{assoc}	S_{cls}	IoU^{St}	IoU^{Th}
<i>(a) IoU-based Association</i>													
4D-PLS [2]	2	-	-	59.9	58.8	61.0	65.0	63.1	-	-	-	-	-
	4	8.0	3.48	62.7	65.1	60.5	65.4	61.3	56.9	56.4	57.4	66.9	51.6
4D-Stop [20]	2	15.9	3.67	66.4	71.8	61.4	64.9	64.1	62.9	67.3	58.8	68.3	53.3
	4	18.9	4.32	67.0	74.4	60.3	65.3	60.9	63.9	69.5	58.8	67.7	53.8
Eq-4D-Stop [67]	2	11.3	2.89	68.9	74.8	63.5	65.7	68.4	65.4	69.7	61.5	68.7	59.1
	4	12.1	3.18	70.1	<u>77.6</u>	63.4	66.4	67.1	67.0	72.0	62.4	69.1	60.9
Mask4Former [58]	2	10.4	3.51	70.5	74.3	66.9	67.1	66.6	<u>68.4</u>	67.3	69.6	72.7	65.3
	4	17.1	8.56	<u>71.9</u>	76.3	67.8	66.9	69.0	68.0	69.7	66.3	70.7	60.3
<i>(c) Detect & Track Association</i>													
GEO-4D (Ours)	1	3.2	2.35	72.7	78.3	67.5	65.2	70.6	70.3	<u>70.0</u>	70.5	72.7	67.4

their relative contributions. By minimizing \mathcal{C} with the Hungarian algorithm [21], we obtain a bijective assignment that considers the geometric alignment. We present experimental results in Section C.3.

C Additional Experimental Results

C.1 Leaderboard Results

Table A.2 shows the SemanticKITTI [4] challenge leaderboard ranks on the hidden test set, ordered by LSTQ. In this leaderboard, we observe that our proposed GEO-4D outperforms not only all published methods but also every competition participant. Specifically, we achieve 1st place in LSTQ as of submission date. These results demonstrate the strong generalization capability and practical effectiveness of our method under challenging scenarios.

C.2 Effect of the Number of Scans.

In Table A.3, we examine how well our proposed GEO-4D performs instance association with only a single scan. The number of superimposed scans is a pivotal factor influencing the association performance of the IoU-based method.

Table A.4: Comparison of the quantitative results on panoptic nuScenes [13].

Model	LSTQ	S_{assoc}	S_{cls}	Thing classes (AQ / IoU)											Stuff classes (IoU only)				
				barrier	bicycle	bus	car	const. veh.	motorcycle	pedestrian	traffic cone	trailer	truck	drive. surf.	other flat	sidewalk	terrain	manmade	vegetation
Mask4Former [58]	67.6	63.0	72.5	48.3/76.9	42.6/37.0	60.5/90.2	76.7/92.7	42.7/44.9	61.1/77.0	53.5/74.0	48.9/55.7	38.7/47.8	62.2/77.8	95.6	69.2	71.5	74.6	88.5	87.0
Mask4D [32]	58.5	54.1	63.1	29.7/64.3	27.8/20.5	60.5/79.2	72.5/83.5	28.5/21.8	52.5/72.0	42.3/65.9	39.5/43.0	19.2/35.2	58.9/71.8	84.2	53.9	64.9	71.3	85.2	84.5
CA-Net [33]	63.4	56.6	71.0	30.1/74.5	31.9/29.1	56.5/88.5	73.3/91.2	38.6/43.2	63.2/78.7	53.6/71.2	34.6/54.6	39.5/48.3	62.1/77.3	95.6	68.4	70.3	72.7	86.7	85.2
Geo-4D (Ours)	67.9	65.0	71.0	40.7/74.5	44.1/29.1	58.9/88.5	80.9/91.2	40.1/43.2	65.9/78.7	67.2/71.2	52.0/54.6	40.6/48.3	65.7/77.3	95.6	68.4	70.3	72.7	86.7	85.2

Table A.5: Ablation on matching strategy.

Method	LSTQ	S_{assoc}	S_{cls}
Hungarian Matching	72.3	77.6	67.5
Greedy Matching	72.7	78.3	67.5

Since formal reports for specific configurations are unavailable, we reproduce the results using official implementation—namely, Eq-4D-Stop [67] with 2 scans and Mask4Former [58] with 4 scans. As clearly observed in Table A.3, leveraging four superimposed scans yields a substantial improvement in S_{assoc} , with a notable sacrifice in computational efficiency. In contrast, we observe that GEO-4D exhibits superior performance, despite the absence of explicit 4D spatio-temporal volume constructed from stacked point clouds. This observation demonstrates that GEO-4D effectively associates instances using only a single scan and a 3D panoptic network, while remaining highly efficient.

C.3 Analysis of Matching Strategy.

In Table A.5, we compare the performance of GEO-4D with one-to-one or greedy matching. The evaluation is done using SemanticKITTI validation set and set all $\gamma_{\{t,r,s\}} = 1$ for the Hungarian matching. We observe that greedy matching surpasses the bijective matching by a small margin in S_{assoc} . We interpret this gap as being caused by segmentation noise, where a single object is often predicted as multiple disjoint segments. In such case, the greedy strategy adapts to this variability, resulting in more robust temporal consistency. However, as segmentation quality improves, bijective matching becomes advantageous for maintaining unique and consistent identities.

C.4 Analysis of Global Geometry-aware Soft Matching.

In the main paper, we argue that the proposed Global Geometry-aware Soft Matching (GGSM) improves the robustness of the matching strategy against noisy measurements and predictions. To isolate the contribution of GGSM, we additionally evaluate its effectiveness on non-rigid point cloud registration benchmarks [27, 28] independent of tracking performance. This allows us to analyze whether GGSM improves geometric correspondence estimation under challenging conditions such as partial overlap, occlusion, and large motion.

Table A.6: Quantitative comparison on 4DMatch-F [28] and 4DLoMatch-F [28].

Method	4DMatch-F				4DLoMatch-F				
	EPE↓	AccS↑	AccR↑	Outlier↓	EPE↓	AccS↑	AccR↑	Outlier↓	Time*
ICP [6]	0.296	2.96	12.06	71.50	0.565	0.14	0.74	90.87	0.10
Sinkhorn [46]	0.308	2.76	8.13	79.86	0.505	0.20	0.86	89.47	3.76
NICP [38]	0.325	6.44	12.10	80.40	0.517	0.18	0.73	92.37	4.80
NSFP [26]	0.265	8.66	18.65	64.96	0.495	0.38	1.56	84.77	39.54
Ours (ICP+GGSM)	0.210	2.51	11.26	62.58	0.431	0.18	1.19	78.80	1.62

* Runtime measured on a single NVIDIA A100.

Baselines. While more advanced baselines exist for non-rigid point cloud registration, we compare against several representative registration methods to better understand the effectiveness of GGSM. Specifically, we include Iterative Closest Point (ICP) [6] as a classical baseline, Sinkhorn-based registration which is closely related to our global geometry association, Non-rigid ICP (NICP) [38] as an extension of ICP for non-rigid registration, and Neural Scene Flow Prior (NSFP) [26] which predicts point-wise motion using neural networks. ICP determines the global rotation and translation parameters, which are designed for rigid transformations. Optimal Transport (OT) [12] iteratively estimates point displacements by optimizing a transport plan via the Sinkhorn-Knopp algorithm [46] and updating point locations according to the gradients of the OT objective. NICP estimates the movement of all points individually rather than relying on a single rigid transformation. We adopt a typical solution that optimizes a deformation graph with regularization constraints to enforce smooth deformations. NSFP optimizes a multilayer perceptron (MLP) to predict point-wise motion by minimizing the Chamfer distance between two point clouds.

Metrics. We adopt widely used metrics to evaluate how well the registered points align with the ground truth. End-Point Error (EPE) measures the average 3D warping error across all points. AccS and AccR represent the percentage of points whose relative errors are below 2.5% and 5.0%, respectively. Outlier denotes the percentage of points whose relative error exceeds 30%. EPE and Outlier evaluate the overall registration performance, while AccS and AccR measure the point-wise accuracy.

Experimental Analysis. As shown in Tab. A.6, two key observations emerge across both 4DMatch-F and 4DLoMatch-F. First, GGSM achieves the lowest EPE and Outlier rates despite relying only on rigid transformations. Although non-rigid methods achieve higher point-wise accuracy (AccS and AccR), they often introduce globally inconsistent deformations, which can degrade the overall geometric alignment. In contrast, GGSM leverages global geometric structure to estimate a coherent transformation, leading to more reliable overall registration performance. Second, GGSM provides a well-balanced trade-off between efficiency and performance. NSFP models point-wise motion by optimizing a neural network for each point coordinate, which offers strong flexibility but incurs significant computational overhead. Moreover, NICP estimates per-vertex deformation parameters through iterative non-rigid optimization, which also limits efficiency.

On the other hand, our GGSM remains computationally efficient as it inherits the efficiency of rigid ICP, resulting in strong overall registration quality by improving geometric consistency.

Takeaway: In this section, we validate the effect of GGSM in a controlled setting by excluding other factors (e.g., rigid objects and driving surface in on-road environments). It is important to note that the primary scope of this work is 4D LiDAR panoptic segmentation in driving scenes, rather than non-rigid point cloud registration itself. These experimental results support our claim that GGSM plays a crucial role in enabling robust and reliable instance association in driving scenes with both rigid and non-rigid instances. For additional discussions, please refer to the corresponding analyses presented in the main manuscript.

C.5 Quantitative Results

We additionally provide the results of each semantic class on panoptic nuScenes [13] to facilitate a more comprehensive understanding. We present our reproduced results obtained from officially given training configurations. Note that 4D-Stop [20] and EQ-4D-Stop [67] do not provide official class-wise results for the panoptic nuScenes benchmark, whereas only overall metrics such as LSTQ are available. For this reason, class-wise comparisons against these methods are excluded to avoid confusion and ensure fairness. In Table A.4, our method yields overall performance improvements, particularly in safety-critical *thing* classes (e.g., bicycle, car, and pedestrian). Furthermore, classes with relatively fewer points, such as pedestrians and traffic cones, exhibit stronger association performance against the baselines. This observation aligns with our earlier analysis on SemanticKITTI [4] presented in the main manuscript.

C.6 Qualitative Results

In this section, we present additional qualitative analysis by illustrating the results of SemanticKITTI [4] and panoptic nuScenes [13] dataset. As clearly shown in Figure A.1 and A.2, GEO-4D maintains robust ID consistency even in challenging scenarios. Our method explicitly incorporates the inherent geometric relations between instances and adopts a delicately designed pipeline that is resilient to occlusion and noisy predictions. In contrast, Mask4Former [58] associates instances by selecting the majority ID among spatially overlapped points, making it vulnerable to imprecise predictions and leading to frequent ID switches (see the 1st, 2nd, and 3rd rows of Figure A.1). Apart from this, Mask4D [32] struggles with separating nearby objects and accumulates errors from early mispredictions (see the 1st, 2nd, and 4th rows of Figure A.1). Furthermore, GEO-4D also operates well on the panoptic nuScenes dataset, which is sparse and large temporal gaps between consecutive scans. Specifically, in the 2nd and 4th rows of Figure A.2, we observe that the instances have no overlap and sparse representations. The baselines confuse the instance IDs due to their partial observations and rapid motions. However, GEO-4D successfully finds the corresponding instances even

when they are distant. Also, from the 1st row of Figure A.2, we observe that GEO-4D can effectively associate instances in complex scene where pedestrians are heavily entangled.

D Discussion

D.1 Limitation and Future work

We identify several limitations of our proposed approach, which inherits issues from both pre-trained 3D panoptic models and LiDAR sensors. While GEO-4D demonstrates strong association performance with a cost efficient pipeline, real-time deployment remains challenging. Our method highly depends on the performance of the underlying 3D panoptic model; thus, its runtime can be further improved as point cloud processing continues to advance. In addition, partial observation of instances in LiDAR sensing make it difficult to reliably associate instances. Incorporating trajectory cues represents a promising direction to further stabilize instance association. Lastly, our pipeline forces the requirement of camera parameters as a prerequisite for transforming the point coordinates into the world coordinates. Relaxing this requirement would improve the applicability of our method in broader real-world settings. We hope these insights encourage continued progress toward scalable 4D perception systems.

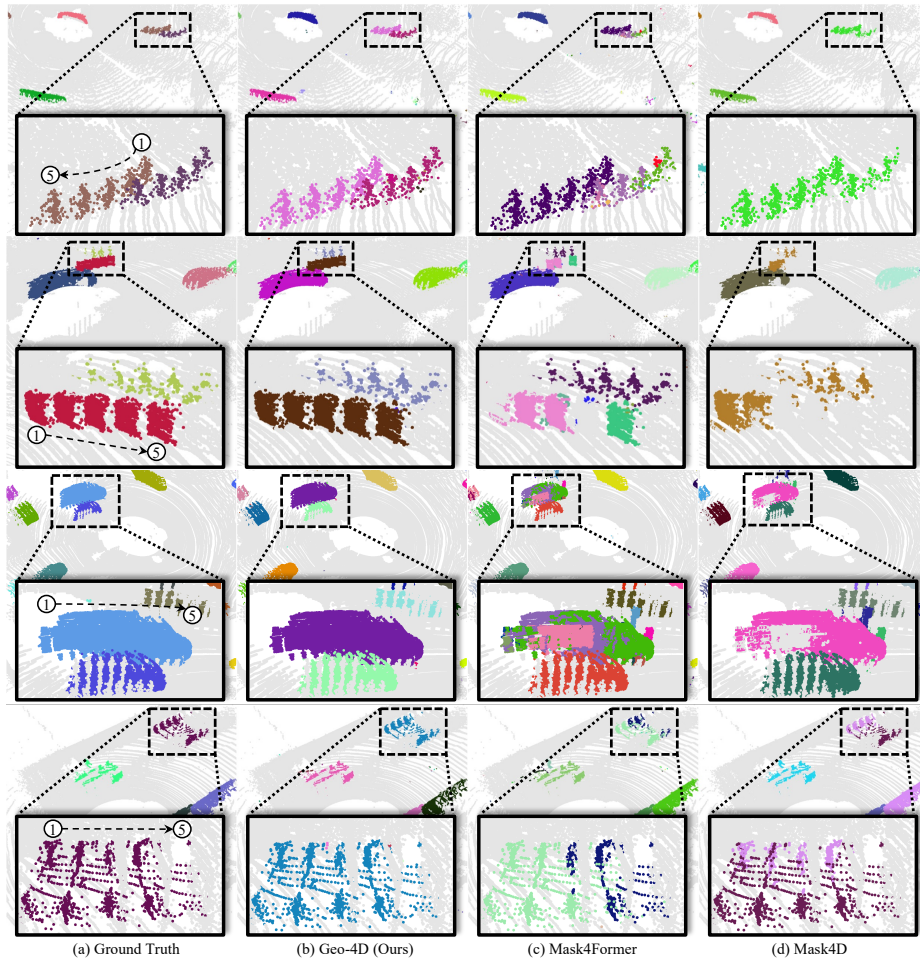


Fig. A.1: Qualitative comparison on semanticKITTI [4] validation set. We visualize the association results over five consecutive scans for both the baselines and our GEO-4D. Different colors represent different instances. The dotted boxes zoom in for clear comparison. For clarity, we use circled numbers (①–⑤) to represent the frame indices.

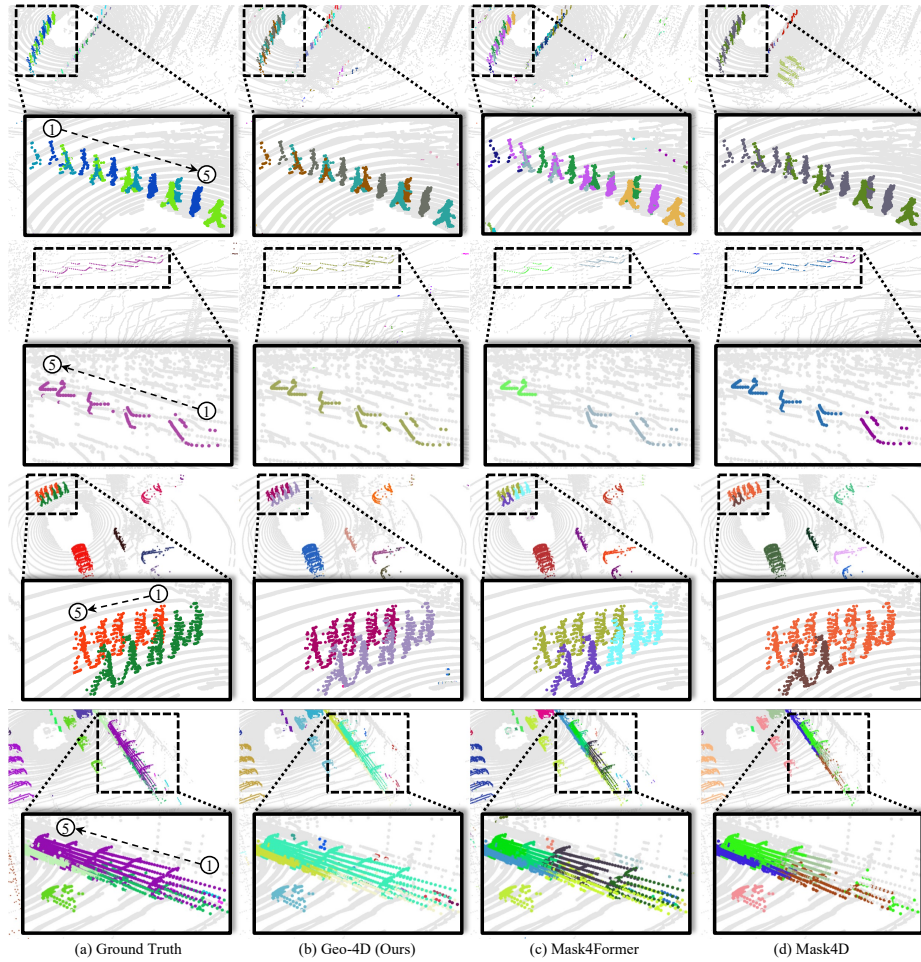


Fig. A.2: Qualitative comparison on panoptic nuScenes [13]. We visualize the association results over five consecutive scans for both the baselines and our GEO-4D. Different colors represent different instances. The dotted boxes zoom in for clear comparison. For clarity, we use circled numbers (①–⑤) to represent the frame indices.